The effect of model tidal forcing on virtual particle dispersion and accumulation at the ocean surface

The effect of model tidal forcing on virtual particle dispersion and accumulation at the ocean surface

Laura Gomez-Navarro[1,1], Erik Van Sebille[1,1], Verónica MORALES MÁRQUEZ[2,2], Ismael Hernandez-Carrasco[3,3], Aurelie Albert[4,4], Clement Ubelmann[5,5], Julien Le Sommer[6,6], Jean-Marc Molines[7,7], and Laurent Brodeau[5,5]

[1]Utrecht University
[2]Institut Méditerranéen d'Océanologie
[3]SOCIB / IMEDEA
[4]Universite Grenoble Alpes /CNRS/IGE
[5]Datlas
[6]Univ. Grenoble Alpes, CNRS, IRD, Grenoble INP, IGE
[7]French National Centre for Scientific Research (CNRS)

November 9, 2023

Abstract

Understanding the pathways of floating material at the surface ocean is important to improve our knowledge on surface circulation and for its ecological and environmental impacts. Virtual particle simulations are a common method to simulate the dispersion of floating material. To advect the particles, ocean models' velocities are usually used, but only recent ones include tidal forcing. Our research question is: What is the effect of tidal forcing on virtual particle dispersion and accumulation at the ocean surface? As inputs we use velocity outputs from eNATL60, a twin simulation with and without tidal forcing. We focus on the Açores Islands region and we find: 1) Surface particles have a larger displacement, but a lower distance travelled with than without tidal forcing 2) Surface accumulation seasonal differences depend on the spatial scale of the ocean structures 3) A greater variability in surface accumulation is present with tidal forcing.

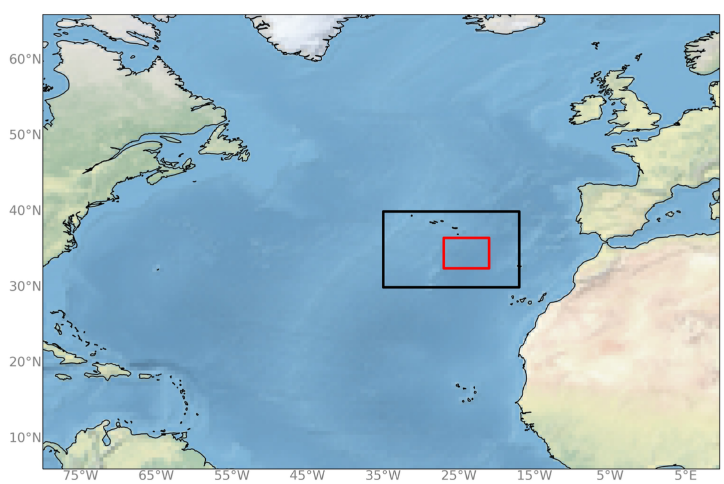

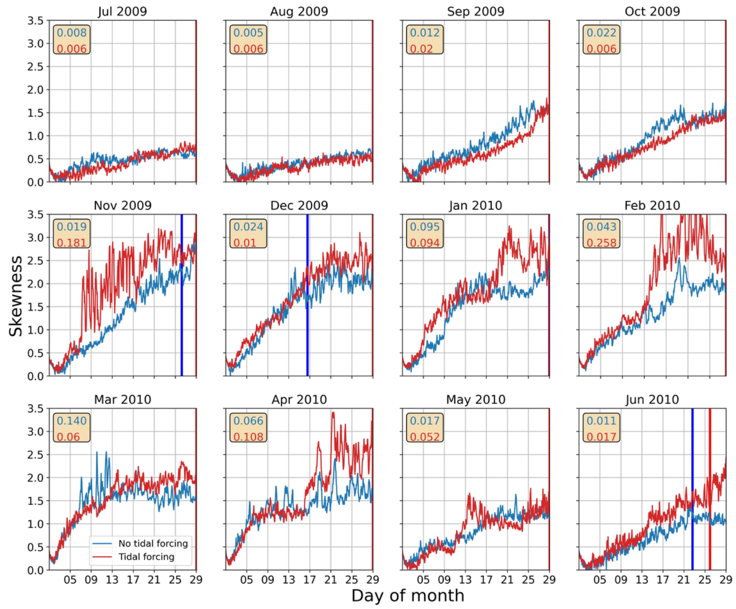

Jul 2009
Aug 2009
Sep 2009
Oct 2009
Nov 2009
Dec 2009
Jan 2010
Feb 2010
Mar 2010
Apr 2010
May 2010
Jun 2010
Skewness
Day of month
No tidal forcing
Tidal forcing

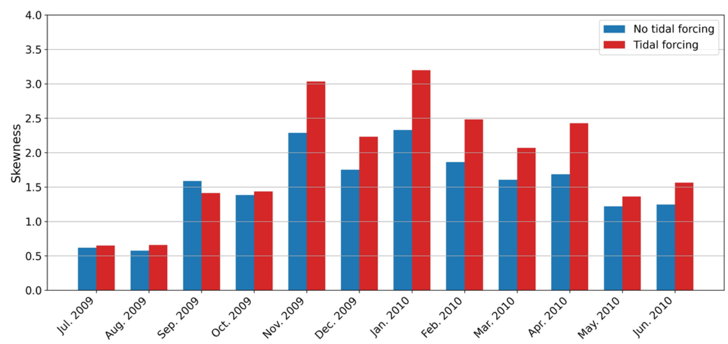

Skewness
No tidal forcing
Tidal forcing
Jul. 2009
Aug. 2009
Sep. 2009
Oct. 2009
Nov. 2009
Dec. 2009
Jan. 2010
Feb. 2010
Mar. 2010
Apr. 2010
May. 2010
Jun. 2010

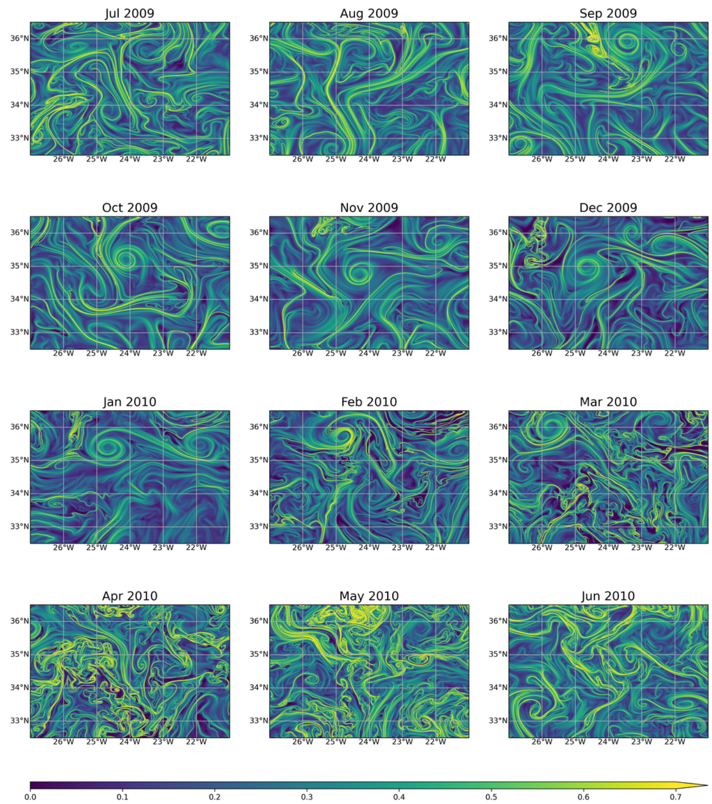
Jul 2009
Aug 2009
Sep 2009
Oct 2009
Nov 2009
Dec 2009
Jan 2010
Feb 2010
Mar 2010
Apr 2010
May 2010
Jun 2010
36°N
35°N
34°N
33°N
26°W 25°W 24°W 23°W 22°W
0.0 0.1 0.2 0.3 0.4 0.5 0.6 0.7

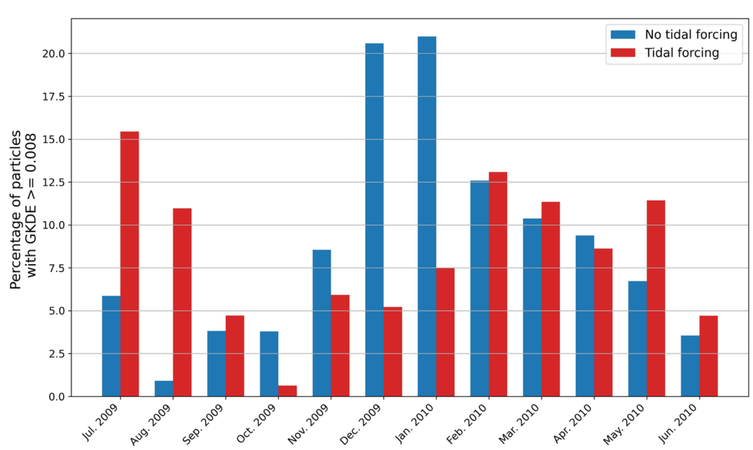
No tidal forcing
Tidal forcing
Percentage of particles with GKDE >= 0.008
0.0 2.5 5.0 7.5 10.0 12.5 15.0 17.5 20.0
Jul. 2009
Aug. 2009
Sep. 2009
Oct. 2009
Nov. 2009
Dec. 2009
Jan. 2010
Feb. 2010
Mar. 2010
Apr. 2010
May. 2010
Jun. 2010

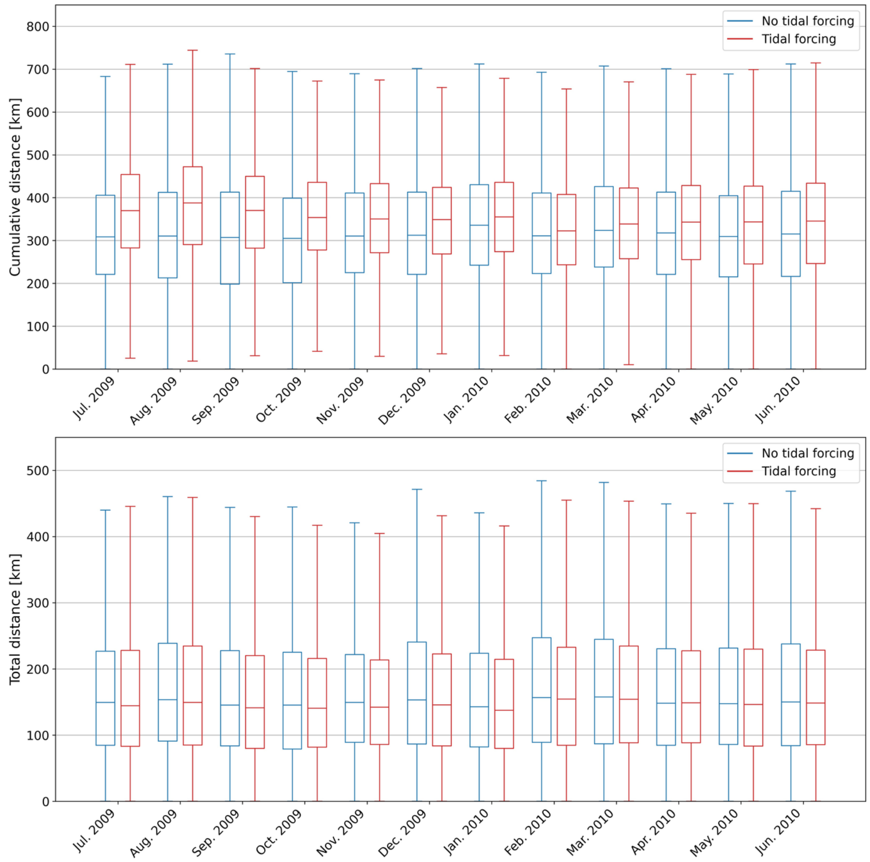

No tidal forcing
Tidal forcing
Cumulative distance [km]
800
700
600
500
400
300
200
100
0
Jul. 2009
Aug. 2009
Sep. 2009
Oct. 2009
Nov. 2009
Dec. 2009
Jan. 2010
Feb. 2010
Mar. 2010
Apr. 2010
May. 2010
Jun. 2010
No tidal forcing
Tidal forcing
Total distance [km]
500
400
300
200
100
0
Jul. 2009
Aug. 2009
Sep. 2009
Oct. 2009
Nov. 2009
Dec. 2009
Jan. 2010
Feb. 2010
Mar. 2010
Apr. 2010
May. 2010
Jun. 2010

The effect of model tidal forcing on virtual particle dispersion and accumulation at the ocean surface

Laura Gómez-Navarro[1], Erik van Sebille[1], Verónica Morales-Marquez[2], Ismael Hernandez-Carrasco[3], Aurelie Albert[4], Clement Ubelmann[5], Julien Le Sommer[4], Jean-Marc Molines[4], Laurent Brodeau[4]

[1]Department of Physics, IMAU, Utrecht University, Utrecht (The Netherlands)
[2]Université de Toulon, Aix Marseille Univ., CNRS, IRD, MIO, Toulon (France)
[3]Mediterranean Institute of Advanced Studies (IMEDEA, UIB-CSIC), Esporles, (Spain)
[4]IGE, UGA-CNRS-IRD-INP, Grenoble (France)
[5]Datlas, Grenoble (France)

Key Points:

- Using velocity outputs from ocean models with tidal forcing affects surface particle dispersion in the region south of the Açores Islands.
- Surface particles have a larger displacement but a lower distance travelled with than without tidal forcing.
- Higher temporal variability and positive skewness of particle density is found, increasing prediction uncertainty of accumulation areas.

Corresponding author: Laura Gómez-Navarro, `l.gomeznavarro@uu.nl`

Abstract

Understanding the pathways of floating material at the surface ocean is important to improve our knowledge on surface circulation and for its ecological and environmental impacts. Virtual particle simulations are a common method to simulate the dispersion of floating material. To advect the particles, ocean models' velocities are usually used, but only recent ones include tidal forcing. Our research question is: What is the effect of tidal forcing on virtual particle dispersion and accumulation at the ocean surface? As inputs we use velocity outputs from eNATL60, a twin simulation with and without tidal forcing. We focus on the Açores Islands region and we find: 1) Surface particles have a larger displacement, but a lower distance travelled with than without tidal forcing 2) Surface accumulation seasonal differences depend on the spatial scale of the ocean structures 3) A greater variability in surface accumulation is present with tidal forcing.

Plain Language Summary

At the surface of the ocean we can find a range of floating material e.g. algae, larvae, plastics and oil spills. Correctly simulating their trajectories is important to understand the ocean surface circulation and their ecological, environmental and economical impacts. To simulate these trajectories, ocean currents data from ocean models are usually used. These ocean models try to represent different oceanic processes, and recent ones include the effect of tides via a tidal forcing. In this study we investigate if tidal forcing affects surface trajectories. Our study region is south of the Açores Islands, where tides have an important impact on surface circulation patterns. We study the distances travelled by particles and how much they accumulate. We find that both the distances travelled and accumulation are affected by tidal forcing. The impacts on the accumulation vary seasonally and depend on the spatial scale of the ocean structures. We conclude that, in this region, using ocean models with tidal forcing is important. Further work needs to be done to know the impact in other ocean regions and to understand the impacts of tidal forcing on ocean surface circulation.

1 Introduction

Understanding the pathways of floating material (e.g. larvae, plastics, oil and drifters) at the surface ocean is important not only due to its ecological and environmental repercussions (Sala et al., 2016), but also to improve our knowledge on the ocean dynamics (van Sebille et al., 2020; Chamecki et al., 2019). These floating material pathways can be studied by analysing horizontal particle dispersion and accumulation. Understanding these 2D surface dynamics also helps to get some insights on the 3d dynamics, by allowing to identify convergence and divergence, and so zones with meaningful vertical motions (e.g., d'Asaro et al., 2018; Hernández-Carrasco et al., 2018; McWilliams et al., 2019; Tarry et al., 2021). Identifying these zones has important implications for biology, by for example, affecting the presence nutrients and phytoplankton (e.g., Lévy et al., 2001). Understanding the surface dispersion and accumulation is not only useful to expand our knowledge on the ocean dynamics, but also for practical issues such as better understanding the distribution of marine plastic (e.g., Onink et al., 2019) and oil spills (e.g., Ainsworth et al., 2021), and algae such as Sargassum (e.g., Miron et al., 2020; van Sebille et al., 2021)) and larvae (e.g., Largier, 2003; Hidalgo et al., 2019; Díaz-Barroso et al., 2022). Identifying spots where floating plastics or fish larvae accumulate, can help ocean clean-up strategies and marine protected areas management, respectively (Krüger et al., 2017).

Simulating accurate trajectories of floating material in the ocean is complex as many processes at different scales are involved (van Sebille et al., 2020). In this regard, the growing development of different sources of ocean velocity data has helped to analyse the impact of different dynamical scales on the transport processes: Ocean General Circulation Models (OGCMs) (e.g., Brunner et al., 2015; Sala et al., 2016), drifters (e.g., Maximenko et al., 2012; van Sebille et al., 2012), High-Frequency (HF) radar (e.g., Hernández-Carrasco et al., 2018; Révelard et al., 2021), altimetric satellite data (e.g., Beron-Vera et al., 2010; Liu et al., 2014) and other products like GlobCurrent (e.g., Onink et al., 2019). Unfortunately, *in situ* and remote sensing data have either a low spatial and/or temporal coverage (drifters and HF radar) or a low spatial resolution (altimetric data). OGCMs are not as limited by coverage and resolution, but to date they cannot resolve and represent all the different processes, like Langmuir circulation, and would need to be coupled to other models, like wave and biogeochemical models, to represent processes such as Stokes drift and bio-fouling, respectively (van Sebille et al., 2020; Tsiaras et al., 2021). Focusing on the open ocean, some of the processes that have received a great attention to improve the understanding of the surface transport properties from observations and numerical simulations, have been Ekman transport, Stokes drift and windage (e.g., Wenegrat & McPhaden, 2016; Iwasaki et al., 2017; Putman et al., 2020; Morales-Márquez et al., 2021; Morales-Márquez et al., Submitted); especially in the context of marine debris (e.g., Maximenko et al., 2018; Dobler et al., 2019; Onink et al., 2019; Higgins et al., 2020). However, little attention has been paid so far to the effect of tides, and even less to the effect of internal waves, on the eddy field and on the Lagrangian dynamics.

In this regard, a few studies have analysed the contribution of tidal induced dynamics to the transport of floating material, and only focused on tidal currents. Sterl et al. (2020) found that the impact of barotropic tidal currents on microplastic surface transport and accumulation was very small. Tidal currents have also been considered using the SMOC dataset (Drillet et al., 2019) to understand the trajectories of *Sargassum* in the Tropical Atlantic by van Sebille et al. (2021). Moreover, the Lagrangian transport due to internal tides has been studied by Sutherland and Yassin (2022), but they found it to be negligible when averaged over an inertial period. Technological advances in the past years have allowed recent OGCMs to include tidal forcing, improving the representation of internal waves and tide fields (Le Sommer et al., 2018). Tidally forced OGCMs allow not only to consider tidal currents, but also the impact tides have on the flow structures, like eddies, filaments, or fronts. To our knowledge, no study looking at the impact of using velocity data from a tidally forced OGCM to simulate surface ocean trajectories has been done before.

Including tidal forcing in OGCMs can impact the flow field in different ways. It increases the energy at the fine-scales (here defined between 10 km and 100 km) as reported in Verron et al. (2020), where a higher Sea Surface Height (SSH) energy level is observed with than without tidal forcing at wavelengths below approximately 100 km. This difference is more pronounced in the northern hemisphere summer (from hereinafter seasons referring to northern hemisphere), when the high stratification conditions promote the generation and propagation of internal tides (Verron et al., 2020). One of the physical features that are responsible for this increase at the fine-scales are internal waves, which are ignored when only considering tidal currents and/or barotropic tides. Although internal waves occur at the interface between ocean layers (Arbic et al., 2018), their signal can sometimes be observed at the ocean surface (e.g., C. Jackson et al., 2012). Not only can they transport floating material (Shanks, 2021), but they can also affect the background flow, namely eddies, by altering their kinetic energy (Mtfller, 1976; Bühler & McIntyre, 2005; Barkan et al., 2017), as internal waves can lead to the extraction of mesoscale energy through dissipation (Barkan et al., 2017). Since mesoscale eddies are able to retain floating material for several days (e.g., d'Ovidio et al., 2013; Condie & Condie, 2016; Limer et al., 2020; Bello-Fuentes et al., 2021), this loss of energy could imply a loss of the coherence their structure and thus of their capacity to accumulate/trap material. While no specific research has been done on the impact of internal waves on the retention capacity of eddies, some studies have been done with surface waves. Dobler et al. (2019); Morales-Márquez et al. (Submitted) found that surface waves created by forcings like the wind and waves can have a significant effect on mesoscale structures like eddies, modifying their shape, and eventually reducing their retention capacity.

Our study region is located south of the Açores Islands, one of the areas in the North Atlantic with the highest internal waves signal (Ray & Zaron, 2016; Savage et al., 2017). These internal waves are generated by the interaction of the flow (tidal or current) with the bathymetry, especially during summer (June to September), when stratification is high (C. R. Jackson & Apel, 2004). Moreover, this area has been found to be important in terms of marine pollution with a high exposure to marine floating debris, which reaches the islands through filaments and eddies generated from the Gulf Stream (Sala et al., 2016; Pham et al., 2020; Cardoso & Caldeira, 2021).

The objective of this paper is to investigate the effect of tidal forcing on the surface dispersion properties. In Section 2 we describe the dataset used and the methods to evaluate the data. Section 3 describes the results obtained and in Section 4 we discuss them and suggest future studies.

2 Data and methods

2.1 The extended North Atlantic simulation at 1/60 ° (eNATL60)

eNATL60 is an extended version of the NATL60 run (see Ajayi et al. (2020); `https://github.com/meom-configurations/NATL60-CJM165`) in which a larger spatial domain is covered. The model's domain includes the North Atlantic basin : from 6°N to 66°N and from 80°W to 9.5°E, together with the whole Mediterranean and Black Seas and the Gulf of Mexico (fig. 1).

With a spatial resolution of 1/60 ° and a model time-step of 40 seconds, the simulation is submesocale permitting (Verron et al., 2020). For the scope of this study, we use the hourly model outputs, and though the model is 3D, we only use the 2D surface velocity fields. Two simulations have been produced with this configuration : a twin experiment without and with tidal forcing (Brodeau, Le Sommer, & Albert, 2020; Brodeau, Sommer, & Albert, 2020). The tidal constituents used are M2, S2, N2, K1, O1 (Brodeau, Sommer, & Albert, 2020), and the presence of tidal forcing allows the conversion of tidal energy into the internal wave field. This conversion happens through the interaction of wave and unbalanced motions, and via flow-topography interactions (Arbic et al., 2018). The simulation timespan is from mid-June 2009 to October 2010 (simulation years, no data assimilation included). Verron et al. (2020) compared the simulation outputs to the altimeter SARAL/Altika, focusing on a spectral comparison with the simulation's surface data. They found that at the large scales (down to approximately 80 km) the model's SSH spatial spectra is very close to that of SARAL/Altika, for both the non-tidal and tidal run. The high frequency motions eNATL60 have been compared to altimetry by Ansong et al. (2020), showing a slight overestimation of SSH variance in the tidally forced run due to no explicit wave drag in the simulation. This set of simulations present an unprecedented opportunity due to its high spatial and temporal resolution, and its twin simulation characteristic with and without tidal forcing.

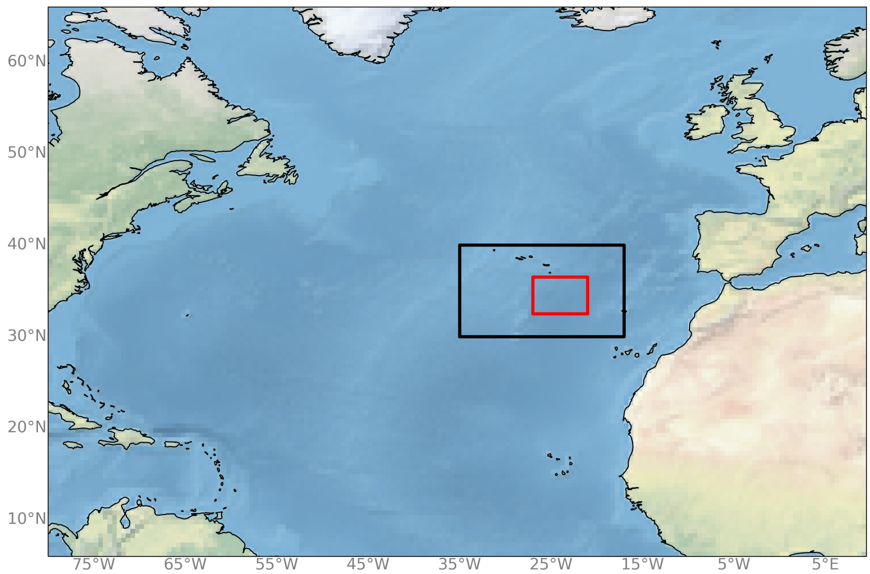

Figure 1. Spatial domain of the eNATL60 simulation. Black box shows the region of this study where virtual surface particles are released. Red box shows the subregion used for some of the analyses.

2.2 Particle trajectory simulations

The OceanParcels Lagrangian framework v2.2.2 (Delandmeter & van Sebille, 2019) is used to simulate 2D trajectories of virtual particles at the sea surface. A fourth order Runge-Kutta particle advection scheme is used with a run-time time-step (dt) of 5 minutes. We consider infinitesimal passive and buoyant particles. Two types of simulations are done. Firstly, particles are released monthly at the surface over the whole region (black box in fig. 1) with a 0.04° spacing, making it a total of 106926 particles. Particles are advected for 28 days, from July 2009 to June 2010. Particles are advected using the velocity field obtained from the outputs of the two model simulations (eNATL60). Particles which leave the domain (black box in fig. 1) are removed. Secondly, in order to calculate backward Finite Time Lyapunov Exponents (bFTLEs), particles are released every 0.004° and advected for 14 days (biweekly). Due to the computational cost, bFTLEs are calculated at the subregion shown in fig. 1 (red box). Further details on the bFTLEs computations and parameterizations are given in Section 2.3.3.

2.3 Diagnostics

To evaluate the impact of tidal forcing on the surface particle trajectories, we use a range of diagnostics that allows us to obtain information at different temporal and spatial scales. We first evaluate the effect of tidal forcing on the flow transport analyzing two Lagrangian properties based on single-particle statistics: the distance travelled by the particles and their surface accumulation. To calculate the distance, we analyse the cumulative and total distances travelled. The analysis of the surface accumulation is more complex and requires different statistical and diagnostic techniques. The surface accumulation diagnostics are sensitive to the choice of different parameters, presenting a higher associated uncertainty than the other metrics based on the travelled distances. We also analyse the impact of the tidal forcing on the transport barriers computing pair of particles metrics like the Finite Time Lyapunov Exponents. Consequently, we use a range of different techniques which are described below.

2.3.1 Gaussian Kernel Density Estimation (GKDE)

One of the methods used to calculate the density of particles is a 2-dimensional horizontal Gaussian Kernel Density Estimation (GKDE). This is a non-parametric (applicable to a non-Gaussian distribution) estimate of the probability density function of a field. The GKDE is applied monthly on all particles in the whole domain (black box in fig. 1) by calculating it on the particle distribution of day 28. We use the python SciPy stats gaussian_kde algorithm with a default kernel size (bandwidth), which is calculated following Scott's Rule (Scott, 1992). This bandwidth selector calculates the optimal bandwidth value that avoids both over-smoothing and under-smoothing.

2.3.2 Particle density histogram skewness

The particle density is also investigated using histograms. A two-dimensional histogram of the particles' monthly positions in the final step is calculated with a bin size of 0.1° by 0.1°. It is calculated for the subregion shown by a red box in fig. 1. This subregion is selected as to avoid regions without particles, which appear as white intrusions and are present in all of the months (for example the white region at the west in the no tides September GKDE subplot of fig. 3). The GKDE is calculated on each particle, so the effect of the region borders is smaller than on the 2D-histogram. Then, a one-dimensional histogram of the number of particles in each bin is calculated from it to show the frequency of the 2D bin counts.

The skewness of the one-dimensional histogram is analysed. This can give us information on the occurrence of extreme events (e.g., White, 1980), and therefore the occurrence of high accumulation zones (i.e., high 2D bin count).

2.3.3 Backward Finite Time Lyapunov Exponents (bFTLEs)

Finite Time Lyapunov Exponents (FTLEs) is a Lagrangian diagnostic for describing local dispersion properties of fluid flows, providing information on the position of oceanic transport barriers, the so-called Lagrangian Coherent Structures (LCS) (Boffetta et al., 2001; Haller, 2015). FTLEs is based on the Lagrangian separation rate of two infinitesimally close trajectories, which grows exponentially over time (Haller, 2001; Shadden et al., 2005). It measures the separation rate of a pair of particles after a fixed time interval (equivalent to Finite Size Lyapunov Exponents (Hernández-Carrasco et al., 2011), which measure the separation rate of two particles, but fixing the final separation distance) (Shadden et al., 2005). Ridges of backward FTLE (bFTLE) fields reveal regions of maximum flow stretching, identifying attracting LCS which act as barriers to transport. Recent studies have shown the relationship between attractive LCS with filaments of accumulated negative Lagrangian horizontal divergence of velocity fields, revealing regions of particle aggregation (Huntley et al., 2015; Hernández-Carrasco et al., 2018).

Based on Shadden et al. (2005), FTLE can be derived considering the stretching of two neighbouring particles, initially separated a distance δ(t0), and advected in the flow after a fixed time of integration (τ), when both particles will be separated $\delta(t_0+\tau)$. We obtain the following expression for the FTLE in two-dimensional flows, denoted as $\lambda(x, y, t)$, which depends on the position and time,

$$\lambda(x, y, t) = \frac{1}{\tau} * ln\frac{\delta(t_0 + \tau)}{\delta(t_0)} \tag{1}$$

Following Shadden et al. (2005), to obtain the FTLEs we compute the maximum eigenvalues of the Cauchy-Green deformation tensor after the integration time (τ) defined in Haller (2001).

The initial particle separation, $\delta(t_0)$, is set to be of 0.004°, which is finer than the eNATL60 grid (0.0167°) and $\tau = 14$ days. This allows a better identification of the subgrid structures present in the bFTLE field, without introducing artifacts (Hernández-Carrasco et al., 2011, 2020). Finally, bFTLEs are calculated biweekly, on day 1 and 15 of each month. A two-weeks integration time was chosen because with $\tau = 28$ days we obtained bFTLE results with a high uncertainty, and for one week of integration time we found that the coherent structures are not fully identified.

3 Results and discussion

Firstly, we look at the impact of tidal forcing on the distance travelled by the particles. We calculate both the cumulative distance travelled (sum of all the distances travelled during each time-step) and the total distance travelled (the shortest distance between the initial and final point of the particle's trajectory). Fig. 2 shows that the particles travel a large range of distances, but if we focus on the median values (fig. 2 box plot percentile 50) we observe differences between the travel distances with and without including tidal forcing. The median cumulative distance values are higher for the tidal than the non-tidal simulation, reaching a 25% increase in August with respect to the non-tidal simulation. This could be explained by the elevated presence of high-frequency motions in the tidal simulation (Verron et al., 2020), making the particles move more and resulting in a longer total particle trajectory. For the median total distance values (fig. 2 (bottom)), the opposite is observed: larger absolute distances are travelled by the particles in the non-tidal than in the tidal simulation. For some months, the non-tidal simulation values of the median are only slightly higher than the tidal values, but the percentile 75 values of most months also reflect this pattern. This suggests that the tidal forcing induces small scale oscillations that increase the displacement of the particles (the cumulative distance) but slightly decreases the total distance travelled.

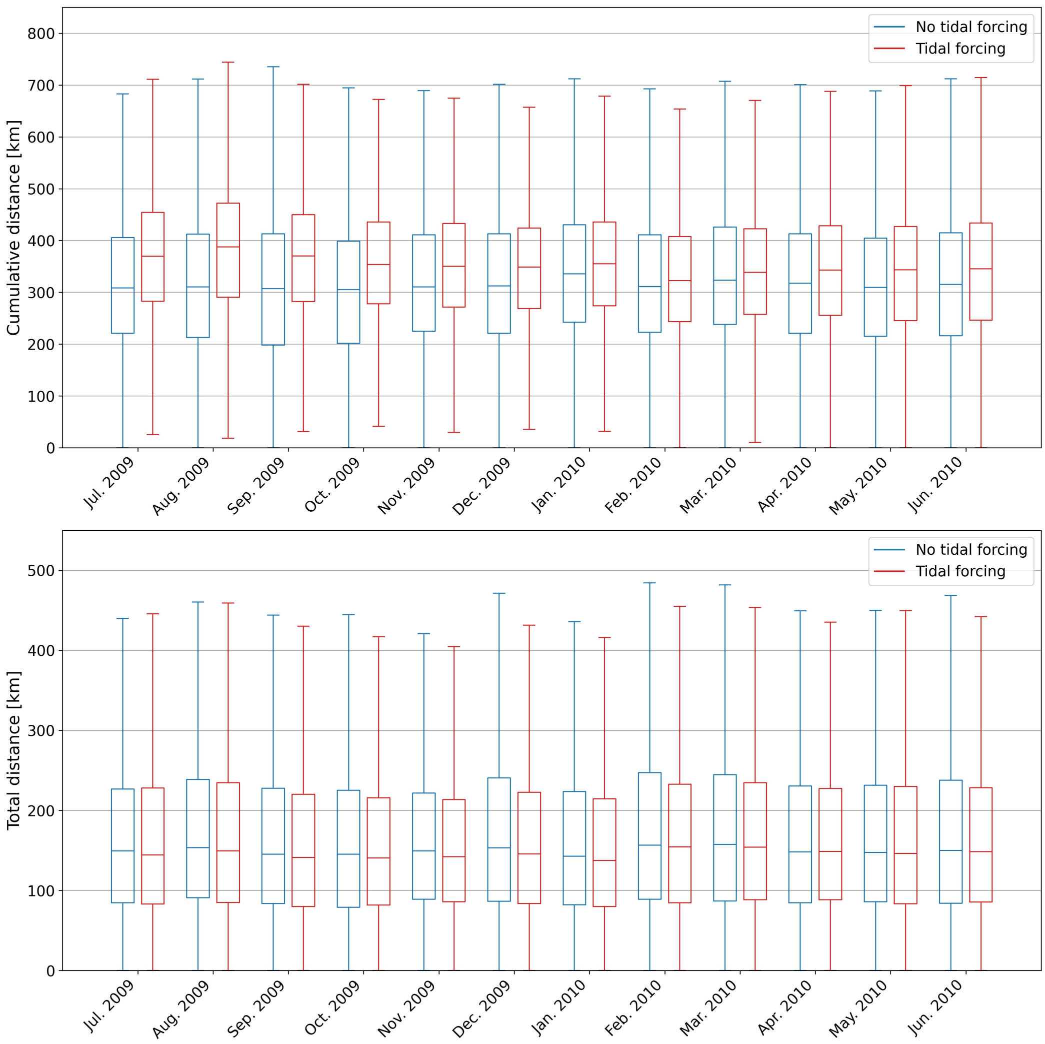

Figure 2. Box plots of mean cumulative distance [km] (top) and mean total distance [km] (bottom) travelled by the virtual particles per month.

Next, we analyse the impact of the tidal induced dynamics on the surface particle accumulation using the GKDE. The results obtained here using the optimal kernel size (see Section 2.3.1), seem to reflect the surface accumulation at mesoscale spatial scales. This can be observed in the red and yellow eddy mesoscale-like structures observed in fig. 3. A higher presence of very high-density regions (red colour) can be observed in winter than in summer, for both simulations (with and without tidal forcing). This implies a higher surface accumulation in winter (December to March) than in summer (July to September 2009 and May and June 2010). This could be due to the higher number of eddies present in winter than in summer and their associated capacity to accumulate floating material (e.g., d'Ovidio et al., 2013; Condie & Condie, 2016; Limer et al., 2020; Bello-Fuentes et al., 2021). A higher presence of eddies in winter than in summer agrees with the higher eddy kinetic energy observed in winter than in summer in this region (Martins et al., 2002).

Secondly, we can observe that this summer-winter difference is lower in the tidally than the non-tidally forced simulation. When tides are included, the accumulation is increased in summer and reduced in winter. Fig. 4 shows the percentage of particles with a high GKDE value (GKDE > 0.008) per month, identified as the yellow and red regions in fig. 3. This corresponds to a GKDE threshold of 0.008, which is value that reflects high particle density for all months in both simulations. In October-December 2009 and January 2010 the percentage of particles with a high GKDE value (high particle density) is reduced between 30% and 84% when tidal forcing is included, while in July-September 2009 and May-June 2010, it is increased between 23% and 1095% (fig. 4). For the rest of the months the increase/decrease is less than 10%.

The increase of GKDE in the summer months could be due to the higher presence of internal waves in the tidally forced simulation, especially in summer when stratification is higher. These internal waves can create more convergence zones (Shanks, 2021). The lower accumulation capacity during winter could be associated with a decrease of the energy at the mesoscale lead by the dissipation effect of internal waves (Barkan et al., 2017). This could reduce the capacity of mesoscale eddies to accumulate surface material, as similarly found to happen with surface waves (Dobler et al., 2019; Morales-Márquez et al., Submitted). On the other hand, the presence of internal waves in winter is lower than in summer. Therefore, the lower accumulation in winter with tidal forcing, could also be explained by the fact that there is more energy at the fine-scales with tidal forcing (Verron et al., 2020), due to the presence of other fine-scale features like submesoscale fronts and filaments. Haza et al. (2016) found that presence of submesoscale structures makes the mesoscale eddy structures more permeable, explaining this lower accumulation with tidal forcing in winter. Overall, the GKDE diagnostic (figs. 3 and 4) shows that including tidal forcing has a clear impact on surface accumulation patterns.

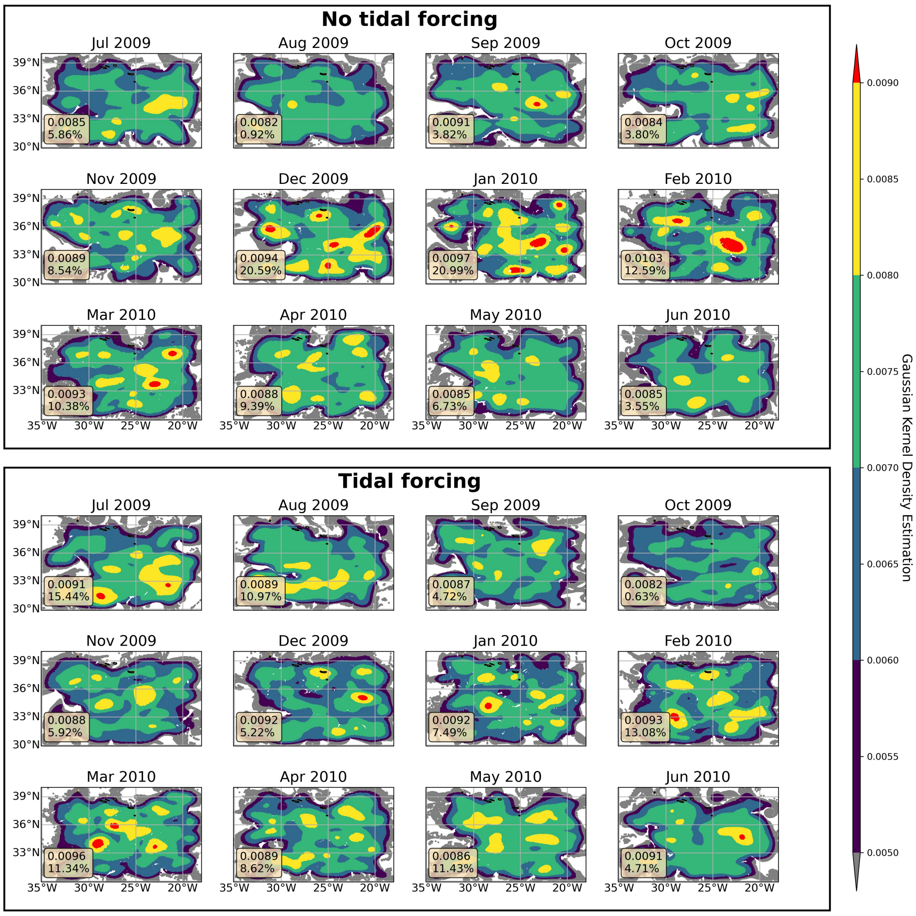

Figure 3. Gaussian kernel density estimation comparison between no tidal forcing (top) and tidal forcing (bottom) simulations. Maximum GKDE value (top) and percentage of particles with a high GKDE value (greater than 0.008) (bottom) are shown in the bottom left textbox.

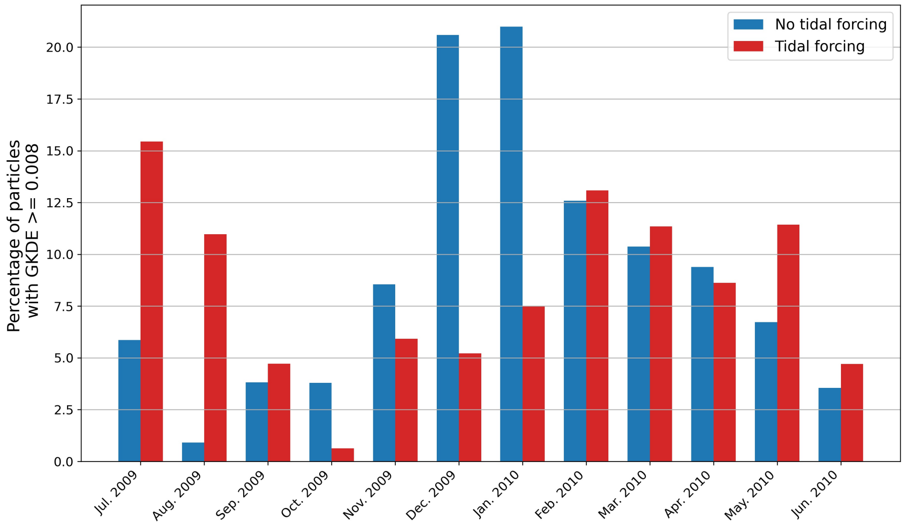

Figure 4. Bar plot comparing the percentage of particles with a high GKDE value (greater than 0.008) per month. Non-tidal results are shown in blue and tidal in red.

To study the surface accumulation from another perspective, 2D-histograms are also analysed. Figure 5 shows the monthly 1D-histograms of the 2D-histogram bin counts of the distribution of the particles in the final time-step. It shows that all the histograms are positively skewed. Qualitatively, no big differences are observed between the non-tidal and tidal histograms. The vertical line in fig. 5 shows the maximum value of the 2D histogram bin counts. The particle density maximum is greater for the tidal than the non-tidal in 7 out of 12 months (August, December, January, February, March, April, and June). No clear pattern is observed in the maximum, though greater values reached in the tidal simulation. This means that zones with much higher accumulation can occur when tidal forcing is included.

We further investigate the positive skewness of the histograms, as it gives us information on the extreme events, which here correspond to the occurrence of a high surface accumulation. Figure 6 (top) shows the temporal evolution of the skewness of the one-dimensional histogram of the particle density (from the two-dimensional histogram) (fig. 5). Both the non-tidal's and tidal's skewness increase with time. The final skewness value is calculated at the time when the first particle released at the boundary of the region (black box fig. 1) enters the subregion (red box fig. 1), and it is represented by the vertical line in fig 5. This done to minimize and homogenize the impact of the

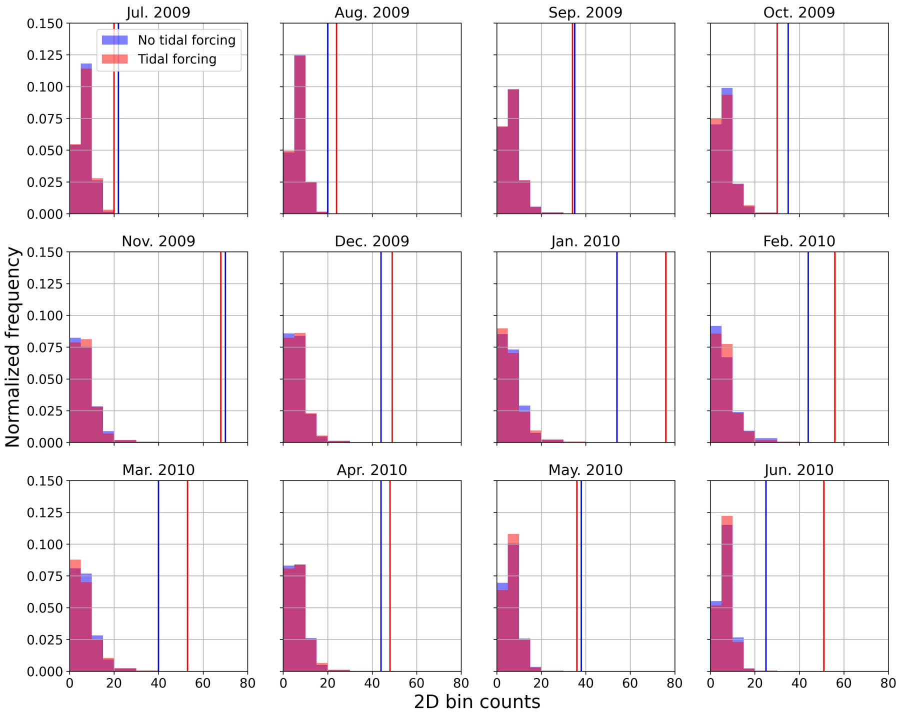

Figure 5. 1D-histogram of the 2D histogram of the distribution of the particles in the final time-step (after 28 days). Results of the non-tidal simulation are shown in blue and from the tidal in red. Vertical lines indicate the maximum value.

simulation boundary effects. The monthly values are shown in the bar plot in fig. 6. Except for September, all months have higher skewness values in the tidal than the non-tidal simulation. For most months, the skewness' temporal variability is highest for the tidal simulation. The temporal variance of the skewness (until the vertical line) is shown in the text boxes in fig 6 (top). For 6 out of the 12 months it is higher for the tidal simulation, in 3 of the months the values are very close (0.002 difference or less) and in the 3 other months it is higher for the non-tidal simulation.

The backward FTLEs give us information on the attracting LCS, identifying transport barriers, and filaments of coherent convergence. It gives us more details at finer scales than the GKDE and the 2D-histograms as it can identify subgrid structures present (see section 2.3.3). Figures 7 and 8 show the bFTLE fields on day 1 of each month for the non-tidal and tidal simulations, respectively. We can observe how eddy structures in the autumn and winter months are much sharper in the non-tidal than tidal simulations. This coincides with the GKDE results in winter. Next, we consider high flow convergence for bFTLE values larger than 0.5 $days^{-1}$. Fig. 9 (top) shows the percentage of particles in the final time-step (after 14 days) with a bFTLE greater than 0.5 $days^{-1}$. For the summer and autumn months (from July to December 2009 and, January and June 2010), non-tidal FTLEs exhibit higher values than the tidal values. During winter and spring, the opposite happens. For both the non-tidal and tidal simulations, the highest percentage of particles with a bFTLE larger than 0.5 is obtained in April, and another smaller peak seems to be present in July. This observed seasonal variability in the bFTLE high values are larger for the tidal than for the non-tidal simulations.

Some differences between GKDE and bFTLE are observed in the months of maximum particle accumulation and in the seasonal variability. While the maximum peak in the GKDE is obtained in January for the non-tidal simulation, the maximum bFTLE is obtained in April and for the tidal simulation. Also, the maximum bFTLE for both simulations is in April, but the maximum GKDE is in different months: January for the non-tidal and July for the tidal simulation. Then, from autumn to winter (October 2009 to March 2010), both for the GKDE and the bFTLE the same relationship between the surface accumulation in the non-tidal and tidal simulations is observed : from October to January the non-tidal is highest, and in February and March the tidal is highest. Then from July to September 2009 and April to June 2010, the relationship between the non-tidal and tidal is opposite in the GKDE and bFTLE fields. These months coincide with the maximum probability of internal waves observation in the Açores Islands (C. R. Jackson & Apel, 2004). Considering that internal waves promote the transfer of energy from the mesoscale to the submesoscale (Barkan et al., 2021), that their presence is more pronounced with tidal forcing, and that bFTLEs capture better the fine-scale and the GKDE the mesoscale transport dynamics; the tidal forcing is affecting differently the FTLE and GKDE diagnostics. We expect then an increase in the bFTLE fields (fine-scales) and a decrease in the GKDE fields (mesoscale) with the tidal forcing simulation. Lastly, it is important to note the different Lagrangian simulation lengths (28 days for GKDE and 14 days for bFTLE) and that a subregion is used for the bFTLE calculation (due to calculation costs) while the GKDE is computed for the whole region. A sensitivity analysis (not shown) of GKDE to different areas was performed, obtaining no significant differences in the resulting accumulation patterns. Therefore, these different Lagrangian simulation characteristics are not responsible for the surface accumulation discrepancies observed between both Lagrangian metrics.

Fig. 9 (bottom) shows the skewness value of the bFTLE 1d-histograms. For most months, it is higher with than without tidal forcing. The only exceptions are from 15/03/2010 to 01/05/2010. This is consistent with the skewness results of the 2D bin counts histograms, and for most months, with the fact that including tidal forcing implies an increase in the positive skewness of the frequency of high surface accumulation areas. Consequently, this means there is a higher occurrence of extreme events (high surface accumulation) with tidal forcing, which could complicate the predictability of surface accumulation regions.

4 Conclusions and perspectives

This study aimed to investigate the impact of using ocean model velocity outputs with tidal forcing on the Lagrangian dynamics. A NEMO North Atlantic twin simulation with a resolution of 1/60° (eNATL60) without and with tidal forcing was used to simulate surface virtual particle trajectories in a region around the Açores Islands. The results show that there is an impact on the ocean surface accumulation and dispersion when tidal forcing is included in OGCMs. This is reflected on the distances travelled by the virtual surface particles, and on the accumulation of particles detected at different scales.

Firstly, when we look at the monthly distances travelled by particles, longer cumulative distances are travelled in the tidal run, but shorter total distances than in the non-tidal run. To analyse the patterns of surface particle density we use three diagnostics: Gaussian Kernel Density Estimation (GKDE), 2D-histograms and backward Finite Time Lyapunov Exponents (bFTLEs). The GKDE analyses seem to represent the mesoscale accumulation, and they show that with tidal forcing, the accumulation increases during the summer months and decreases in the winter months. The 1-dimensional histograms of the particle density (2-dimensional bin counts) show that all monthly distributions are positively skewed. We look at the temporal evolution of this skewness, and we find a high temporal variability, especially for the tidal forcing simulation. After one month, the skewness is higher for the tidal than the non-tidal forcing simulation for all months, except for September. Lastly, we calculate the bFTLEs which can be used as a proxy of convergence flow structures and capture smaller scale dynamics than the previous techniques. We find that in summer, the simulation without tides has a higher percentage of particles with higher bFTLE values than the tidal simulation. For the winter months, the opposite is obtained, except for January. We find that the skewness of the bFTLE 1d-histograms is also higher for the tidal than the non-tidal simulation for all months. Therefore, adding tidal forcing can create a higher occurrence of extreme events, that in this case correspond to regions of high surface particle accumulation.

Several explanations could be behind these results. Barkan et al. (2021) found that when internal wave forcing was used in their simulations (which could be analogous to the tidal forcing used here, as it creates a higher presence of internal waves), less mesoscale kinetic energy is present both in summer and winter. The energy is transferred towards submesoscale fronts and filaments, particularly in winter (Barkan et al., 2021), and this could impact on the coherence of the mesoscale eddies, reducing their capacity to trap particles in a higher presence of submesoscale structures (Haza et al., 2016). This effect could explain the results obtained in winter, especially the opposite effect observed in winter for the GKDE (representative of eddy accumulation) and backward FTLE (more representative of accumulation at fronts and filaments) results.

Further investigation is needed to better understand all the effects of the tidal forcing induced dynamics on the transport and mixing properties. The impact of the fine-scales, and especially unbalanced motions like internal waves, on ocean surface dynamics is currently still being studied (Shakespeare & McC. Hogg, 2018; Thomas & Daniel, 2021; Gula et al., 2022). Future work could look further into this by analysing the impact of the different temporal and spatial scales on the Lagrangian dynamics.

In this study we were limited by the timespan of the eNATL60 simulation, so we were able to analyse data for only one year. It would be interesting to investigate the interannual variability of the tidal effects obtained as there is an EKE interannual variability in this region (Martins et al., 2002). When new model simulations allow it, it would be useful to reproduce this study over longer time periods than the one-year outputs we were limited to here. Also, to fully understand the impacts of tidal forcing found here, it would be relevant to repeat this in other regions, with a lower internal waves signal (e.g., eastern part of the North Atlantic basin, or the Gulf Stream region) and with a higher impact of tidal currents (e.g. the North Sea).

Lastly, in order to focus on Lagrangian trajectory studies around archipelagos and coastal regions, it would be interesting to study the impact of tidal forcing on the arrival (Sala et al., 2016) and beaching (e.g. Yoon et al., 2010; Kaandorp et al., 2020) of virtual particles and the connectivity between islands (Vaz et al., 2013). It would also be interesting to study its impact on the surface-ocean connectivity timescales at a global scale (Jönsson & Watson, 2016). These have important impacts on the understanding of the biodiversity and pollution threats, especially on islands, and the consequent strategies necessary for their protection.

5 Open Research

Details on the model data used in this study, eNATL60, and its availability can be found here `https://github.com/ocean-next/eNATL60` (Brodeau, Le Sommer, & Albert, 2020). The codes used to generate the Lagrangian simulations and analyse them can be found here: `https://github.com/OceanParcels/Azores_TidalForcing`.

Acknowledgments

LGN and EvS were partly funded by the European Research Council (ERC) under the European Union Horizon 2020 research and innovation programme (grant agreement No 715386) and the ESA World Ocean Circulation project, ESA Contract No. 4000130730/20/INB. EvS was also partly supported through the IMMERSE project from the European Union Horizon 2020 Research and Innovation Program (grant agreement no. 821926). VMM was supported by the MORHOC'H2 project, funded by the French "Agence Nationale de la Recherche" and "Direction Générale de l'Armement", grant number 21-ASM1-0003.

Data Availability Statement

References

Ainsworth, C. H., Chassignet, E. P., French-McCay, D., Beegle-Krause, C. J., Berenshtein, I., Englehardt, J., … Zheng, Y. (2021). Ten years of modeling the

Deepwater Horizon oil spill. *Environmental Modelling & Software*, *142*, 105070. doi: 10.1016/j.envsoft.2021.105070

Ajayi, A., Le Sommer, J., Chassignet, E., Molines, J.-M., Xu, X., Albert, A., & Cosme, E. (2020). Spatial and Temporal Variability of the North Atlantic Eddy Field From Two Kilometric-Resolution Ocean Models. *Journal of Geophysical Research: Oceans*, *125*(5), e2019JC015827. doi: 10.1029/2019JC015827

Ansong, J. K., Arbic, B. K., Menemenlis, D., Wallcraft, A. J., Bourdalle-Badie, R., Chanut, J., ... others (2020). Importance of damping in comparison of internal tides in several global hydrodynamical models with altimetry. In *Ocean sciences meeting 2020.*

Arbic, B. K., Alford, M. H., Ansong, J. K., Buijsman, M. C., Ciotti, R. B., Farrar, J. T., ... others (2018). Primer on global internal tide and internal gravity wave continuum modeling in HYCOM and MITgcm. *New frontiers in operational oceanography*, 307–392. Retrieved from `https://www.godae.org/~godae-data/School/Chapter13_Arbic_et_al.pdf`

Barkan, R., Srinivasan, K., Yang, L., McWilliams, J. C., Gula, J., & Vic, C. (2021). Oceanic Mesoscale Eddy Depletion Catalyzed by Internal Waves. *Geophysical Research Letters*, *48*(18), e2021GL094376. doi: 10.1029/2021GL094376

Barkan, R., Winters, K. B., & McWilliams, J. C. (2017). Stimulated imbalance and the enhancement of eddy kinetic energy dissipation by internal waves. *Journal of Physical Oceanography*, *47*(1), 181–198.

Bello-Fuentes, F. J., García-Nava, H., Andrade-Canto, F., Durazo, R., Castro, R., & Yarbuh, I. (2021). Tiempo de retención y capacidad de transporte de los remolinos del noroeste del golfo de México. *Ciencias Marinas*, *47*(2), 71–88. (Number: 2) doi: 10.7773/cm.v47i2.3116

Beron-Vera, F. J., Olascoaga, M. J., & Goni, G. J. (2010). Surface Ocean Mixing Inferred from Different Multisatellite Altimetry Measurements. *Journal of Physical Oceanography*, *40*(11), 2466–2480. doi: 10.1175/2010JPO4458.1

Boffetta, G., Lacorata, G., Redaelli, G., & Vulpiani, A. (2001). Detecting barriers to transport: A review of different techniques. *Physica D: Nonlinear Phenomena*, *159*(1-2), 58–70. doi: 10.1016/S0167-2789(01)00330-X

Brodeau, L., Le Sommer, J., & Albert, A. (2020). *eNATL60 dataset.* Retrieved from https://github.com/ocean-next/eNATL60 doi: 10.5281/zenodo.4032732

Brodeau, L., Sommer, J. L., & Albert, A. (2020). *eNATL60: Material describing the set-up and the assessment of NEMO-eNATL60 simulations.* Zenodo. Retrieved from https://doi.org/10.5281/zenodo.4032732 doi: 10.5281/zenodo.4032732

Brunner, K., Kukulka, T., Proskurowski, G., & Law, K. L. (2015). Passive buoyant tracers in the ocean surface boundary layer: 2. observations and simulations of microplastic marine debris. *Journal of Geophysical Research: Oceans*, *120*(11), 7559–7573.

Bühler, O., & McIntyre, M. E. (2005). Wave capture and wave–vortex duality. *Journal of Fluid Mechanics*, *534*, 67–95.

Cardoso, C., & Caldeira, R. M. A. (2021). Modeling the Exposure of the Macaronesia Islands (NE Atlantic) to Marine Plastic Pollution. *Frontiers in Marine Science*, *8*, 332. doi: 10.3389/fmars.2021.653502

Chamecki, M., Chor, T., Yang, D., & Meneveau, C. (2019). Material Transport in the Ocean Mixed Layer: Recent Developments Enabled by Large Eddy Simulations. *Reviews of Geophysics*, *57*(4), 1338–1371. (_eprint: https://agupubs.onlinelibrary.wiley.com/doi/pdf/10.1029/2019RG000655) doi: 10.1029/2019RG000655

Condie, S. A., & Condie, R. (2016). Retention of plankton within ocean eddies. *Global Ecology and Biogeography*. doi: 10.1111/geb.12485

Delandmeter, P., & van Sebille, E. (2019). The Parcels v2.0 Lagrangian framework: new field interpolation schemes. *Geoscientific Model Development*, *12*(8), 3571–3584. (Publisher: Copernicus GmbH) doi: 10.5194/gmd-12-3571-2019

Dobler, D., Huck, T., Maes, C., Grima, N., Blanke, B., Martinez, E., & Ardhuin, F. (2019). Large impact of Stokes drift on the fate of surface floating debris in the South Indian Basin. *Marine Pollution Bulletin*, *148*, 202–209. doi: 10.1016/j.marpolbul.2019.07.057

Drillet, Y., Chune, S. L., Levier, B., & Drevillon, M. (2019). Smoc: a new global surface current product containing the effect of the ocean general circulation, waves and tides. In *Geophysical research abstracts* (Vol. 21).

Díaz-Barroso, L., Hernández-Carrasco, I., Orfila, A., Reglero, P., Balbín, R., Hidalgo, M., ... Alvarez-Berastegui, D. (2022, March). Singularities of surface mixing activity in the Western Mediterranean influence bluefin tuna larval habitats. *Marine Ecology Progress Series*, *685*, 69–84. doi: 10.3354/meps13979

d'Asaro, E. A., Shcherbina, A. Y., Klymak, J. M., Molemaker, J., Novelli, G., Guigand, C. M., ... others (2018). Ocean convergence and the dispersion of flotsam. *Proceedings of the National Academy of Sciences*, *115*(6), 1162–1167.

d'Ovidio, F., Monte, S. D., Penna, A. D., Cotté, C., & Guinet, C. (2013). Ecological implications of eddy retention in the open ocean: a Lagrangian approach. *Journal of Physics A: Mathematical and Theoretical*, *46*(25), 254023. Retrieved 2021-10-17, from `https://iopscience.iop.org/article/10.1088/1751-8113/46/25/254023/meta` (Publisher: IOP Publishing) doi: 10.1088/1751-8113/46/25/254023

Gula, J., Taylor, J., Shcherbina, A., & Mahadevan, A. (2022). Chapter 8 - Submesoscale processes and mixing. In M. Meredith & A. Naveira Garabato (Eds.), *Ocean Mixing* (pp. 181–214). Elsevier. doi: 10.1016/B978-0-12-821512-8.00015-3

Haller, G. (2001). Distinguished material surfaces and coherent structures in three-dimensional fluid flows. *Physica D: Nonlinear Phenomena*, *149*(4), 248–277. doi: 10.1016/S0167-2789(00)00199-8

Haller, G. (2015). Lagrangian Coherent Structures. *Annu. Rev. Fluid Mech*, *47*, 137–162. doi: 10.1146/annurev-fluid-010313-141322

Haza, A. C., Özgökmen, T. M., & Hogan, P. (2016). Impact of submesoscales on surface material distribution in a gulf of Mexico mesoscale eddy. *Ocean Modelling*, *107*, 28–47. doi: 10.1016/j.ocemod.2016.10.002

Hernández-Carrasco, I., Alou-Font, E., Dumont, P.-A., Cabornero, A., Allen, J., & Orfila, A. (2020). Lagrangian flow effects on phytoplankton abundance and composition along filament-like structures. *Progress in Oceanography*, *189*, 102469. doi: 10.1016/j.pocean.2020.102469

Hernández-Carrasco, I., López, C., Hernández-García, E., & Turiel, A. (2011). How reliable are finite-size Lyapunov exponents for the assessment of ocean dynamics? *Ocean Modelling*, *36*(3-4), 208–218. doi: 10.1016/j.ocemod.2010.12.006

Hernández-Carrasco, I., Orfila, A., Rossi, V., & Garçon, V. (2018). Effect of small scale transport processes on phytoplankton distribution in coastal seas. *Scientific Reports*, *8*(1), 8613. doi: 10.1038/s41598-018-26857-9

Hidalgo, M., Rossi, V., Monroy, P., Ser-Giacomi, E., Hernández-García, E., Guijarro, B., ... Reglero, P. (2019). Accounting for ocean connectivity and hydroclimate in fish recruitment fluctuations within transboundary metapopulations. *Ecological Applications*, *29*(5), e01913. doi: 10.1002/eap.1913

Higgins, C., Vanneste, J., & Bremer, T. S. (2020). Unsteady Ekman-Stokes Dynamics: Implications for Surface Wave-Induced Drift of Floating Marine Litter. *Geophysical Research Letters*, *47*(18), e2020GL089189. doi: 10.1029/2020GL089189

Huntley, H. S., Lipphardt Jr., B. L., Jacobs, G., & Kirwan Jr., A. D. (2015). Clusters, deformation, and dilation: Diagnostics for material accumulation regions. *Journal of Geophysical Research: Oceans*, *120*(10), 6622–6636. doi: 10.1002/2015JC011036

Iwasaki, S., Isobe, A., Kako, S., Uchida, K., & Tokai, T. (2017). Fate of microplastics and mesoplastics carried by surface currents and wind waves: A numerical model approach in the Sea of Japan. *Marine Pollution Bulletin*, *121*(1), 85–96. doi: 10.1016/j.marpolbul.2017.05.057

Jackson, C., da Silva, J., & Jeans, G. (2012). The Generation of nonlinear internal waves. *Oceanography*, *25*(2), 108–123. doi: http://dx.doi.org/10.5670/oceanog.2012.46

Jackson, C. R., & Apel, J. (2004). An atlas of internal solitary-like waves and their properties. *Contract*, *14*(03-C), 559.

Jönsson, B. F., & Watson, J. R. (2016). The timescales of global surface-ocean connectivity. *Nature Communications*, *7*(1), 11239. doi: 10.1038/ncomms11239

Kaandorp, M. L., Dijkstra, H. A., & van Sebille, E. (2020). Closing the Mediterranean Marine Floating Plastic Mass Budget: Inverse Modeling of Sources and Sinks. *Environmental Science and Technology*, *54*(19), 11980–11989. (Publisher: American Chemical Society) doi: 10.1021/acs.est.0c01984

Krüger, L., Ramos, J., Xavier, J., Grémillet, D., González-Solís, J., Kolbeinsson, Y., ... others (2017). Identification of candidate pelagic marine protected areas through a seabird seasonal-, multispecific-and extinction risk-based approach. *Animal Conservation*, *20*(5), 409–424.

Largier, J. L. (2003). Considerations in Estimating Larval Dispersal Distances from Oceanographic Data. *Ecological Applications*, *13*(sp1), 71–89. doi: 10.1890/1051-0761(2003)013[0071:CIELDD]2.0.CO;2

Le Sommer, J., Chassignet, E. P., & Wallcraft, A. J. (2018). Ocean Circulation Modeling for Operational Oceanography: Current Status and Future Challenges. *New frontiers in operational oceanography*, 289–306. doi: 10.17125/gov2018.ch12.289

Lévy, M., Klein, P., & Treguier, A.-M. (2001). Impact of sub-mesoscale physics on production and subduction of phytoplankton in an oligotrophic regime. *Journal of marine research*, *59*(4), 535–565.

Limer, B. D., Bloomberg, J., & Holstein, D. M. (2020). The influence of eddies on coral larval retention in the flower garden banks. *Frontiers in Marine Science*. doi: 10.3389/fmars.2020.00372

Liu, Y., Weisberg, R. H., Vignudelli, S., & Mitchum, G. T. (2014). Evaluation of altimetry-derived surface current products using Lagrangian drifter trajectories in the eastern Gulf of Mexico. *Journal of Geophysical Research: Oceans*, *119*(5), 2827–2842. (Publisher: Blackwell Publishing Ltd) doi: 10.1002/2013JC009710

Martins, C. S., Hamann, M., & Fiúza, A. F. G. (2002). Surface circulation in the eastern North Atlantic, from drifters and altimetry. *Journal of Geophysical Research: Oceans*, *107*(C12), 10–1–10–22. doi: 10.1029/2000JC000345

Maximenko, N., Hafner, J., Kamachi, M., & MacFadyen, A. (2018). Numerical simulations of debris drift from the Great Japan Tsunami of 2011 and their verification with observational reports. *Marine Pollution Bulletin*, *132*, 5–25. doi: 10.1016/j.marpolbul.2018.03.056

Maximenko, N., Hafner, J., & Niiler, P. (2012). Pathways of marine debris derived from trajectories of Lagrangian drifters. *Marine Pollution Bulletin*, *65*. (ISBN: 0025-326X) doi: 10.1016/j.marpolbul.2011.04.016

McWilliams, J. C., Gula, J., & Molemaker, M. J. (2019). The gulf stream north wall: Ageostrophic circulation and frontogenesis. *Journal of Physical Oceanography*, *49*(4), 893–916.

Miron, P., Olascoaga, M. J., Beron-Vera, F. J., Putman, N. F., Triñanes, J., Lumpkin, R., & Goni, G. J. (2020). Clustering of Marine-Debris- and *Sargassum*

-Like Drifters Explained by Inertial Particle Dynamics. *Geophysical Research Letters*, *47*(19). doi: 10.1029/2020GL089874

Morales-Márquez, V., Hernández-Carrasco, I., Fox-Kemper, B., & Orfila, A. (Submitted). Ageostrophic contribution by the wind and waves induced flow to the lateral stirring in the mediterranean sea. *Journal of Physical Oceanography*. doi: 10.31223/X56D25

Morales-Márquez, V., Hernández-Carrasco, I., Simarro, G., Rossi, V., & Orfila, A. (2021). Regionalizing the Impacts of Wind- and Wave-Induced Currents on Surface Ocean Dynamics: A Long-Term Variability Analysis in the Mediterranean Sea. *Journal of Geophysical Research: Oceans*, *126*(9), e2020JC017104. doi: 10.1029/2020JC017104

Mtfller, P. (1976). On the diffusion of momentum and mass by internal gravity waves. *Journal of Fluid Mechanics*, *77*(4), 789–823.

Onink, V., Wichmann, D., Delandmeter, P., & van Sebille, E. (2019). The role of ekman currents, geostrophy, and stokes drift in the accumulation of floating microplastic. *Journal of Geophysical Research: Oceans*, *124*(3), 1474–1490.

Pham, C. K., Pereira, J. M., Frias, J. P. G. L., Ríos, N., Carriço, R., Juliano, M., & Rodríguez, Y. (2020). Beaches of the Azores archipelago as transitory repositories for small plastic fragments floating in the North-East Atlantic. *Environmental Pollution*, *263*, 114494. doi: 10.1016/j.envpol.2020.114494

Putman, N. F., Lumpkin, R., Olascoaga, M. J., Trinanes, J., & Goni, G. J. (2020, August). Improving transport predictions of pelagic Sargassum. *Journal of Experimental Marine Biology and Ecology*, *529*, 151398. doi: 10.1016/j.jembe.2020.151398

Ray, R. D., & Zaron, E. D. (2016). M2 Internal Tides and Their Observed Wavenumber Spectra from Satellite Altimetry. *Journal of Physical Oceanograph*, *46*(1), 3–22. doi: 10.1175/JPO-D-15-0065.1

Révelard, A., Reyes, E., Mourre, B., Hernández-Carrasco, I., Rubio, A., Lorente, P., … Tintoré, J. (2021). Sensitivity of Skill Score Metric to Validate Lagrangian Simulations in Coastal Areas: Recommendations for Search and Rescue Applications. *Frontiers in Marine Science*, *8*, 191. doi: 10.3389/fmars.2021.630388

Sala, I., Harrison, C. S., & Caldeira, R. M. (2016). The role of the azores archipelago in capturing and retaining incoming particles. *Journal of Marine*

Systems, *154*, 146-156. doi: https://doi.org/10.1016/j.jmarsys.2015.10.001

Savage, A. C., Arbic, B. K., Richman, J. G., Shriver, J. F., Alford, M. H., Buijsman, M. C., ... others (2017). Frequency content of sea surface height variability from internal gravity waves to mesoscale eddies. *Journal of Geophysical Research : Oceans*, *122*(3), 2519–2538.

Scott, D. W. (1992). *Multivariate density estimation: theory, practice, and visualization.* John Wiley & Sons Inc., New York, USA. doi: 10.1002/9780470316849

Shadden, S. C., Lekien, F., & Marsden, J. E. (2005). Definition and properties of Lagrangian coherent structures from finite-time Lyapunov exponents in two-dimensional aperiodic flows. *Physica D: Nonlinear Phenomena*, *212*(3-4), 271–304. doi: 10.1016/j.physd.2005.10.007

Shakespeare, C. J., & McC. Hogg, A. (2018). The Life Cycle of Spontaneously Generated Internal Waves. *Journal of Physical Oceanography*, *48*(2). (ISBN: 9789048133321) doi: 10.1175/JPO-D-17-0153.1

Shanks, A. L. (2021). Observational evidence and open questions on the role of internal tidal waves on the concentration and transport of floating plastic debris. *Frontiers in Marine Science*, *8*, 633. doi: 10.3389/fmars.2021.621062

Sterl, M. F., Delandmeter, P., & van Sebille, E. (2020). Influence of barotropic tidal currents on transport and accumulation of floating microplastics in the global open ocean. *Journal of Geophysical Research: Oceans*, *125*(2), e2019JC015583.

Sutherland, B. R., & Yassin, H. (2022, October). The nonlinear evolution of internal tides. Part 2. Lagrangian transport by periodic and modulated waves. *Journal of Fluid Mechanics*, *948*, A22. doi: 10.1017/jfm.2022.690

Tarry, D. R., Essink, S., Pascual, A., Ruiz, S., Poulain, P.-M., Özgökmen, T., ... others (2021). Frontal convergence and vertical velocity measured by drifters in the alboran sea. *Journal of Geophysical Research: Oceans*, *126*(4), e2020JC016614.

Thomas, J., & Daniel, D. (2021). Forward flux and enhanced dissipation of geostrophic balanced energy. *Journal of Fluid Mechanics*, *911*. (Publisher: Cambridge University Press) doi: 10.1017/jfm.2020.1026

Tsiaras, K., Hatzonikolakis, Y., Kalaroni, S., Pollani, A., & Triantafyllou, G. (2021). Modeling the Pathways and Accumulation Patterns of Micro- and Macro-

Plastics in the Mediterranean. *Frontiers in Marine Science*, *8*, 1389. doi: 10.3389/fmars.2021.743117

van Sebille, E., Aliani, S., Law, K. L., Maximenko, N., Alsina, J. M., Bagaev, A., ... others (2020). The physical oceanography of the transport of floating marine debris. *Environmental Research Letters*, *15*(2), 023003.

van Sebille, E., England, M. H., & Froyland, G. (2012). Origin, dynamics and evolution of ocean garbage patches from observed surface drifters. *Environmental Research Letters*, *7*(4), 044040. Retrieved 2021-10-17, from https://doi.org/10.1088/1748-9326/7/4/044040 (Publisher: IOP Publishing) doi: 10.1088/1748-9326/7/4/044040

van Sebille, E., Zettler, E., Wienders, N., Amaral-Zettler, L., Elipot, S., & Lumpkin, R. (2021). Dispersion of surface drifters in the tropical atlantic. *Frontiers in Marine Science*, *7*, 1243. doi: 10.3389/fmars.2020.607426

Vaz, A. C., Richards, K. J., Jia, Y., & Paris, C. B. (2013). Mesoscale flow variability and its impact on connectivity for the island of Hawai'i. *Geophysical Research Letters*, *40*(2), 332–337. doi: 10.1029/2012GL054519

Verron, J., Bonnefond, P., Andersen, O., Ardhuin, F., Bergé-Nguyen, M., Bhowmick, S., ... Zaron, E. (2020). The SARAL / AltiKa mission : A step forward to the future of altimetry. *Advances in Space Research*. Retrieved from https://doi.org/10.1016/j.asr.2020.01.030 doi: 10.1016/j.asr.2020.01.030

Wenegrat, J. O., & McPhaden, M. J. (2016). Wind, Waves, and Fronts: Frictional Effects in a Generalized Ekman Model. *Journal of Physical Oceanography*, *46*(2), 371–394. doi: 10.1175/JPO-D-15-0162.1

White, G. H. (1980). Skewness, Kurtosis and Extreme Values of Northern Hemisphere Geopotential Heights. *Monthly Weather Review*, *108*(9), 1446–1455. (Publisher: American Meteorological Society Section: Monthly Weather Review) doi: 10.1175/1520-0493(1980)108⟨1446:SKAEVO⟩2.0.CO;2

Yoon, J.-H., Kawano, S., & Igawa, S. (2010). Modeling of marine litter drift and beaching in the Japan Sea. *Marine Pollution Bulletin*, *60*(3), 448–463. doi: 10.1016/j.marpolbul.2009.09.033

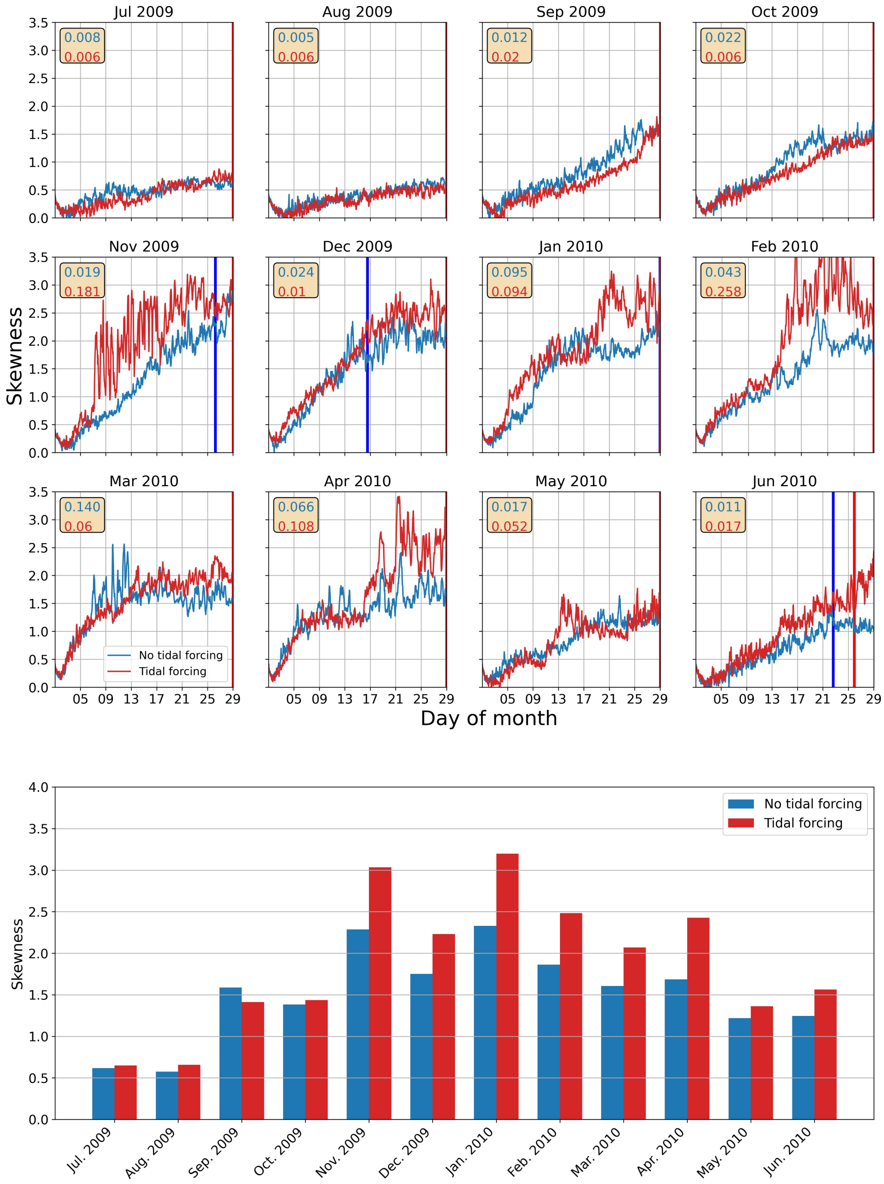

Figure 6. Skewness temporal evolution in time for each month for non-tidal (blue) and tidal (red) simulations. Values in the text box are the variance of the skewness from the beginning of the month till the vertical line. The vertical line indicates the moment in time when the first particle enters the subregion (see subsection 2.3.2). Bottom plot shows the skewness value at the vertical line.

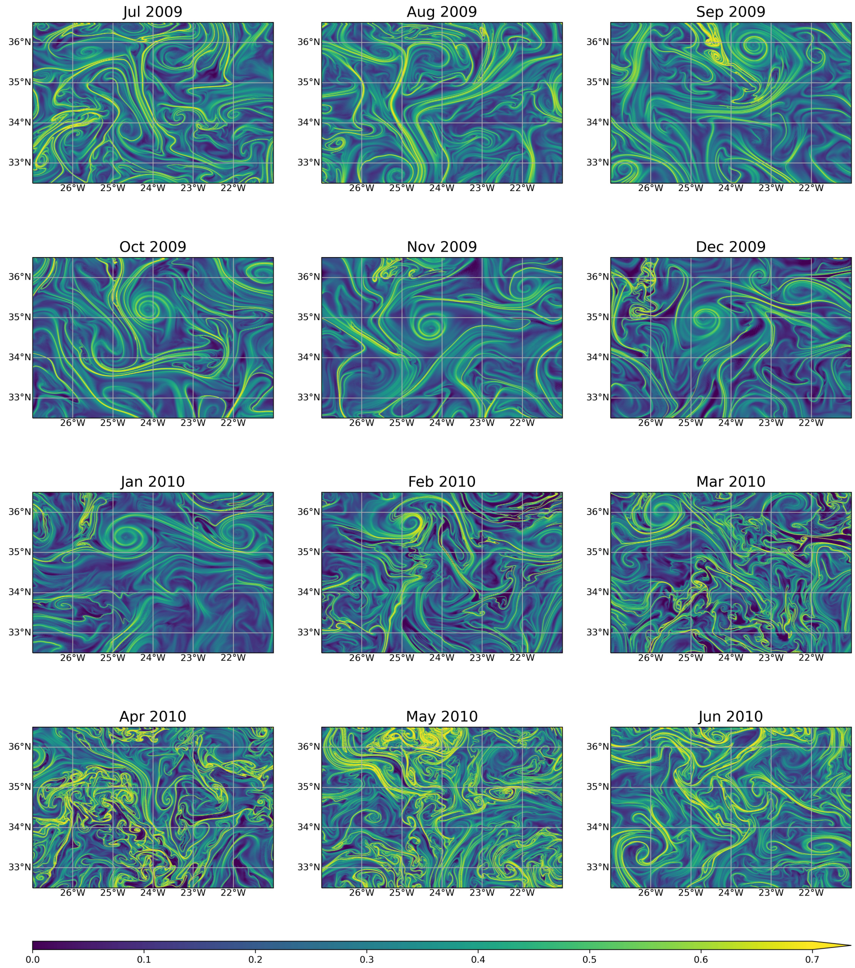

Figure 7. Backward FTLE $days^{-1}$ on day 01 of each month for the no tidal forcing simulation.

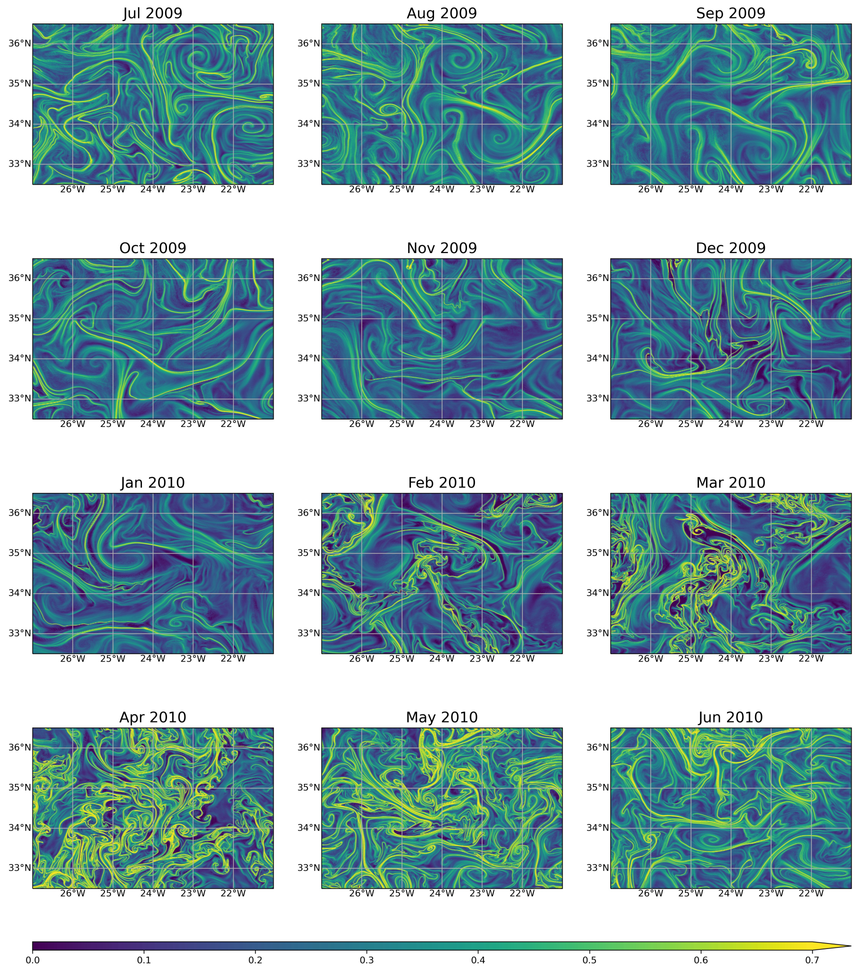

Figure 8. Backward FTLE $days^{-1}$ on day 01 of each month for the tidal forcing simulation.

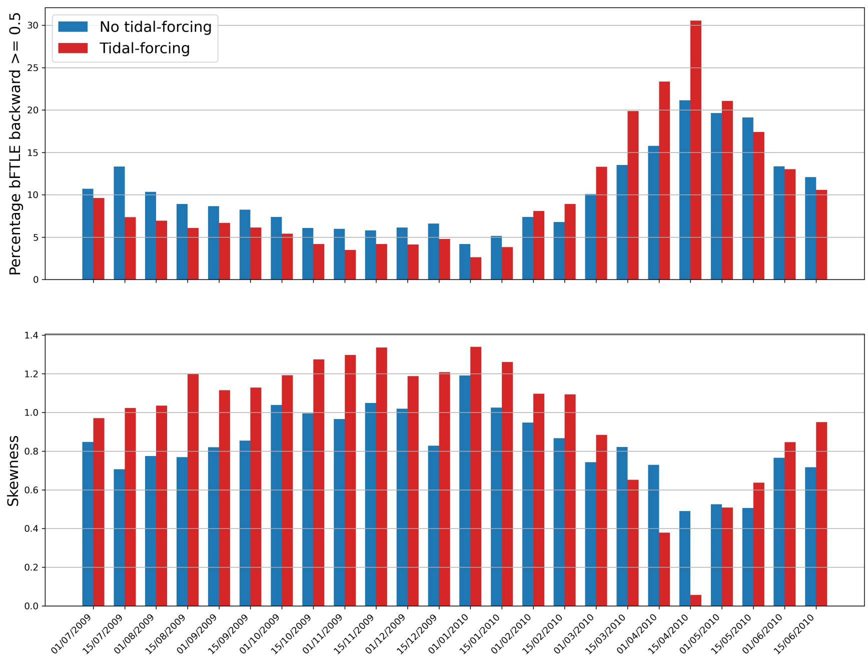

Figure 9. Top: Percentage of virtual particles with backward FTLE > 0.5 $days^{-1}$. Bottom: Skewness values of the backward FTLE one-dimensional histogram.